



The effect of explosions in road tunnels on critical structural elements

Downloaded from: <https://research.chalmers.se>, 2024-04-10 19:00 UTC

Citation for the original published paper (version of record):

Peterson, V., Lozano Mendoza, F., Johansson, M. et al (2023). The effect of explosions in road tunnels on critical structural elements. Expanding Underground - Knowledge and Passion to Make a Positive Impact on the World- Proceedings of the ITA-AITES World Tunnel Congress, WTC 2023: 3263-3271. <http://dx.doi.org/10.1201/9781003348030-395>

N.B. When citing this work, cite the original published paper.

The effect of explosions in road tunnels on critical structural elements

V. Peterson

KTH Royal Institute of Technology, Div. of Concrete Structures, Stockholm, Sweden

F. Lozano

Chalmers University of Technology, Div. of Structural Engineering, Gothenburg, Sweden

M. Johansson

Chalmers University of Technology, Div. of Structural Engineering/Norconsult AB, Gothenburg, Sweden

M. Hallgren

KTH Royal Institute of Technology, Div. of Concrete Structures/Tyréns AB, Stockholm, Sweden

A. Ansell

KTH Royal Institute of Technology, Div. of Concrete Structures, Stockholm, Sweden

J. Magnusson

The Swedish Fortifications Agency, Eskilstuna, Sweden

ABSTRACT: In the present paper, the walls of a concrete frame used for over-decking in a road tunnel were first designed using the relevant design provisions. The response of the wall was then analysed using non-linear finite element analysis, and the results of the finite element analysis were compared to what was predicted using the design guidelines. Additionally, simulations of the blast load resulting from gas leakage during transportation were conducted as a separate study. The results from two vapour clouds containing gases of hydrogen and propane were compared.

1 INTRODUCTION

The Swedish Transport Administration uses its developed design provisions for road tunnels in Sweden; see the Swedish Transport Administration (2021). It states that road tunnels subjected to accidental loads should be designed such that failure of the tunnel components does not initiate a progressive collapse of the load-bearing structure, but local damage is accepted. Possible accidental loads are e.g. collision loads, and blast loads due to explosions resulting from the ignition of vapour clouds or explosive charges. However, the loads in the design provisions do not cover the transport of dangerous substances, for such cases a separate inquiry must be conducted.

Transport on roads of combustible substances such as liquefied petroleum gas (LPG) or hydrogen is common, and the possible accidental explosion of such substances has had detrimental consequences, as reported by Strehlow (1998). During a spill of e.g. LPG, the liquid vaporize and mix with the air as it disperses. If the mixture is within the flammability limits, ignition within the cloud may initiate and propagate a flame front due to the combustion process. Generally, the ignition of a completely unconfined and uncongested vapour cloud would result in a weak deflagration, causing a flash fire and slight overpressures which would be relieved by

expansion, see van der Berg (1985). However, confinement limits the free expansion of the flow and facilitates flame acceleration which could result in severe deflagrations, and possibly a deflagration to detonation transition (DDT), as described by Oran et al. (2020). This implies that significant blast loads may occur in road tunnels from the confinement of the tunnel walls and congestion from traffic in case a vapour cloud ignites. Another important factor determining the resulting blast is the reactivity of the combustible, as described by Bjerkevedt et al. (2000).

This paper aims primarily to study the response of the concrete frame subjected to the load from an internal explosion described in the design provisions using the finite element analysis software Abaqus FEA, documented by Dassault Systèmes (2014). This response is then compared to what was predicted using the guidelines for design. Additionally, possible blast loads arising from gas explosions of hydrogen and propane are then determined using computational fluid dynamics (CFD) simulations with FLACS-CFD, documented by Gexcon AS (2022), and compared with current design provisions. The simulations of the response using Abaqus and of the gas explosions using FLACS-CFD were conducted as two separate studies on the same tunnel configuration.

2 CASE STUDIED

Based on the demands given by the Swedish Transport Administration (2021), a concrete tunnel consisting of a frame structure was chosen as it has appropriate critical elements that must be analysed. This principle is used in e.g. the road over-decking in Hagastaden in Sweden, and the dimensions of the elements presented in Figure 1(a) are deemed to be representative of a concrete frame used for over-decking. This work is limited to focusing on the response of the walls.

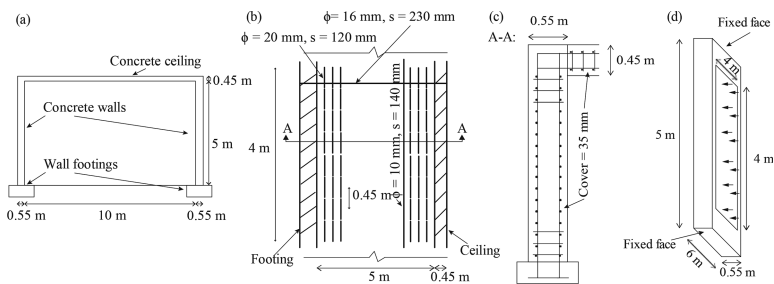


Figure 1. (a) Dimensions of the elements in the frame structure; (b) reinforcement for the wall and ceiling; section showing the wall thickness, ceiling thickness and cover; and (d) the idealized case used for design of the reinforcement.

The reinforcement in the concrete wall was designed using the old Swedish design provisions for impulse-loaded structures (von Essen 1973), as this describes a design procedure. The new acting provisions, i.e. FKR 2011 (Swedish Fortification Agency 2011), were then used to verify the design. The load used was the pressure on a local area presented in Table 1, where P^+ is the peak overpressure and t^+ its duration. The concrete was assumed to be of grade C30/37 with a reinforcement of grade B500C. For design, the concrete wall was assumed to work as a fixed-fixed plate strip with a 6 m width. This equivalent width was determined approximately using the principle of an equivalent width for wide flanges in T-beams described by CEN (2005). The plate strip spans 5 m, only carrying the load in one direction, between the ceiling and the wall footing. A schematic illustration of the idealized case used is presented in Figure 1(d). The reinforcement amounts resulting from the calculations are presented in Figure 1(b) and (c), where ϕ is the reinforcement diameter and s the reinforcement spacing. According to the design provisions used, there was a need for shear reinforcement as the concrete and flexural reinforcement alone was not enough to resist the shear force due to the support reaction determined using the Swedish Fortification Agency (2011). The effect of adding the shear reinforcement was investigated in the discussions.

According to the literature study, hydrogen and propane spills are considered to be the most likely sources of vapour clouds in tunnels, and hence, stoichiometric mixtures of both gas types are also evaluated in this study. The case is presented in Figures 2(a) and (b). The minimum lane requirements for tunnel highways described by the Swedish Transport Administration (2020) were used to construct the plane view in Figure 2(a). Three rows of idealized cars are placed symmetrically around the lane separation line. The confined vapour cloud volume fills the entire cross-section over the space of the three rows of cars, which results in a cloud volume of approximately 1000 m³. The cloud is ignited at a point 0.175 m above the floor.

Table 1. Design loads of explosion in a tunnel, Swedish Transport Administration (2021).

Case	P^+ [kPa]	t^+ [ms]
Local pressure on a 4×4 m ² area in the traffic space	5000	2
Uniform pressure in the traffic space	100	50

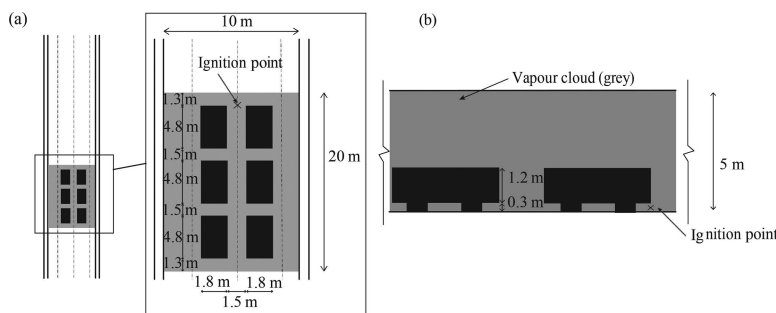


Figure 2. (a) Plane view showing the vehicle configuration; and (b) elevation view.

3 NUMERICAL MODELS

3.1 FEM-models for the response

The FEM-models were analyzed in Abaqus using an explicit solver, and the load applied consisted of the local pressure prescribed in Table 1. The tunnel was assumed to behave as an infinitely long tunnel, i.e. without any reflection of the incident waves in the length direction due to the boundary conditions. The symmetry plane in the length direction was utilized as shown in Figure 3(a), meaning that only half of the tunnel length was modelled. The bottom face was restrained by a multi-point constraint (MPC) in all degrees of freedom (DOF) for the loaded wall (facilitating determination of the total reaction forces on the face from only one node) and the entire bottom face was restrained in all DOF for the adjacent wall. Only the darker grey areas in Figure 3(a) were assumed to crack, and they were modelled using the concrete damage plasticity model (CDPM). The tension softening curve used in the CDPM model was assumed to have an exponential shape (see Cornellisen et al. 1986) using the equation for the fracture energy proposed in FIB (2013), and the compression curve followed the non-linear equation in CEN (2005). The lighter grey areas were modelled using a linear elastic material model to reduce computational demand. This assumption was verified by studying the strains in post-processing; the strains in the area modelled with elastic material did not reach the crack limit. An average 0.1 m mesh consisting of linear brick elements using reduced integration and enhanced hourglass control was applied as shown in Figure 3(a), and infinite elements were used in the length direction. The use of infinite elements results in no need to model the entire tunnel length due to their absorption of the incident waves. Figure 3(a) shows that only the part

modelled with non-linear concrete contained reinforcement. The reinforcement was modelled with 0.1 m linear truss elements, assuming perfect bond to the surrounding concrete, and the material model consisted of a plasticity part and a ductile damage formulation. The simplified bi-linear relation for the stress and strain formulated in FIB (2013) was used for the reinforcement. The chosen finite elements, material model properties and modelling procedure were based on the study by Mathern and Yang (2021). Mean material properties were used for the concrete; compressive strength $f_{cm} = 38$ MPa, tensile strength $f_{ctm} = 2.9$ MPa and Young's modulus $E_{cm} = 33$ GPa, and characteristic material properties were used for the reinforcement; yield strength $f_{yk} = 500$ MPa, tensile strength $f_{tk} = 1.15f_{yk}$ and strain at maximum force $\varepsilon_{uk} = 7.5\%$ (see CEN 2005). The same properties were used for design.

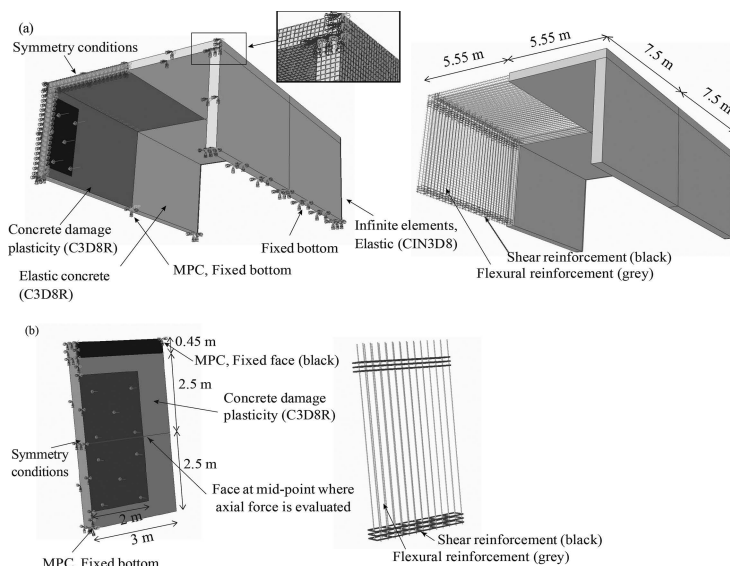


Figure 3. Main characteristics of the non-linear models; (a) frame model and (b) plate-strip model.

The simplified model used for the design in Figure 1(c) was also modelled as shown in Figure 3(b), denoted as the plate-strip (PS) model. This was done so that design considerations could be compared to the results of the frame model described above. The PS model was constructed using the same element types, material models and loading as the frame model. However, the dimensions and boundary conditions were different. The vertical face where the wall connects to the ceiling and the horizontal bottom face where the wall connects to the wall footing was fully restrained in all DOF using an MPC for one model (model denoted "FEA PS Vertical Restraints"). These boundary conditions are an idealisation of the restraining effect from the ceiling. The restraint on the vertical DOF was lifted in another model to remove the restraint on in-plane translation due to the ceiling (model denoted "FEA PS No Vertical Restraints"). Both models were herein analysed to deduce the effect of the in-plane restraint from the ceiling on the response of the wall as it is not considered in design.

3.2 Model used for the gas explosion analyses

The same tunnel configuration was used for the gas explosion analyses using the FLACS-CFD code. Only a segment of the tunnel with a length of 160 m was modelled to reduce computational demand. This limited length was verified to not induce disturbance of the pressure levels within the core domain due the boundary conditions. Plane-wave boundary conditions were used in the inplane directions at the domain boundaries, as shown in Figure 4 where the

model is described, and these are non-reflective. The tunnel walls, ceiling and ground as well as the vehicles were assumed to be rigid and fixed. Two vapour cloud mixtures were analyzed; one stoichiometric air-hydrogen gas mixture (i.e. 30% hydrogen gas H_2 , 70% air), and one stoichiometric air-propane mixture (i.e. 4% propane, 96% air). The two mixtures were compared to deduce the effect of the reactivity of the cloud. The initial turbulent characteristics were considered by a characteristic velocity of $U_0 = 10$ m/s, and relative turbulent intensity of $I_t = 10$ %. The cell size in the core domain of the model was 0.05 m; i.e. 6 cells were used to solve the flow beneath each vehicle. This domain spans a length of 70 m, and outside the core domain, the cells were gradually increased in size towards the boundaries to reduce computational demand. The main characteristics of the model are presented in Figure 4. Three monitor points were positioned at the mid-point of one of the tunnel walls, at distances from the ignition point $R = 20$, $R = 26$, and $R = 36$ m, respectively. The first monitor point is located 1 m outside the vapour cloud. The cars were placed symmetrically in the tunnel.

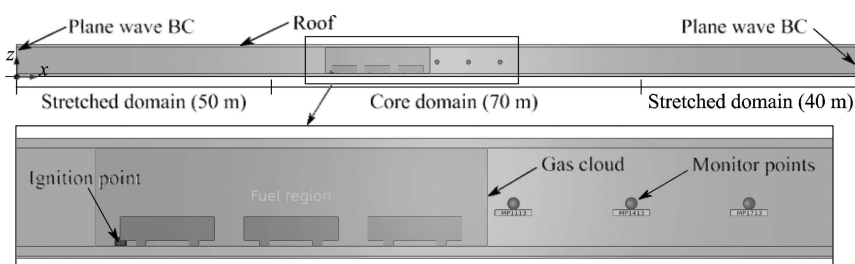


Figure 4. Main characteristics of the model used to simulate the vapour cloud explosions.

4 RESULTS AND DISCUSSION

4.1 Results from response analyses

The simple plate strip model used for design in Figure 1(c) was translated into an equivalent single-degree of freedom (SDOF) model using the procedure described in Biggs (1964). The equivalent SDOF-system method was applied as it is equivalent to the method used to develop the design provisions by the Swedish Fortification Agency (2011) as explained by Magnusson (2019). In Figure 5(a), the displacement of the frame model containing shear reinforcement (FEA Frame S) and the model containing no shear reinforcement (FEA Frame NS) showed to be equivalent. This indicates that the shear reinforcement was not utilized in the wall. This conclusion is supported by Figure 7(c), where no plastic deformation occurs in the shear reinforcement of the frame model. The shear force used for design is determined by the support reaction, and the variation of the support reaction in time for the models is shown in Figure 5(b). The SDOF model shows an instantaneously occurring support reaction, with an amplitude that is approximately 1.7 times larger than the maximum reaction determined in the FEA models. The reason for the divergence in results is that it takes time for the support reaction to develop in the wall due to its inertia, which is not considered in the SDOF model. The SDOF model may therefore produce over-conservative support reactions for load cases with durations that are small in relation to the wave propagation velocity of the structural element.

In Figure 5(a), the analysed frame models shows smaller maximum displacements than the SDOF-model used for design. This shows that the design procedure used is too conservative; the frame structure showed a maximum displacement significantly smaller than the displacement capacity. This discrepancy between the SDOF-model based on a one-way spanning plate-strip and the frame model owes is due to the plate action, and also membrane forces developing in the wall of the frame. The reason for occurrence of membrane forces is the in-plane restraints from the wall footing and inertia of the ceiling. The nodal forces normal to the cross-section in the mid-point of the loaded wall in the frame model were added together to determine the

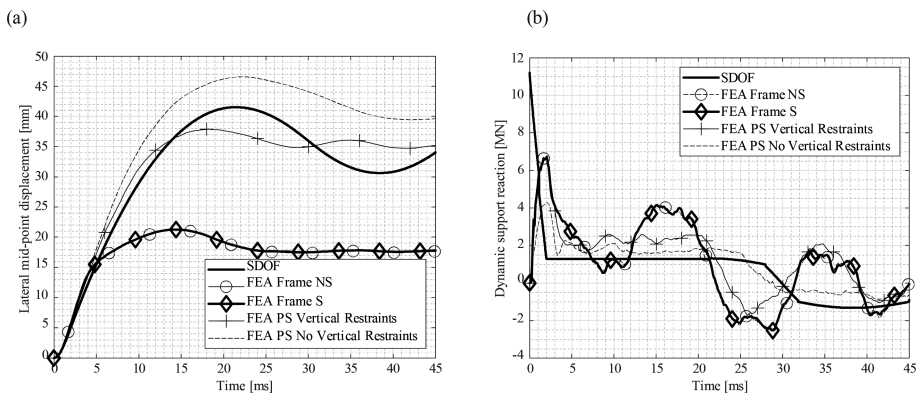


Figure 5. (a) Displacement over time for the SDOF model, frame model and PS models; and (b) dynamic reaction force.

membrane force variation over time in Figure 6. The membrane force is initially tensile (positive), before becoming compressive (negative), after which large tensile forces are sustained.

Deducing whether the plate action or membrane forces resulted in too conservative results of the SDOF-model used for design was carried out by comparing the PS models to the frame models in Figure 5(a). The PS models result in larger maximum displacements than the frame models, and the maximum displacements of the PS models show to be similar to what was predicted using the SDOF model. Although large axial forces develop for mainly the PS model with the vertical restraint in Figure 6, the response is still not comparable the frame model. This shows that it is mainly plate action, and not the developed axial forces, that leads to over-conservative results of the SDOF-model used for design.

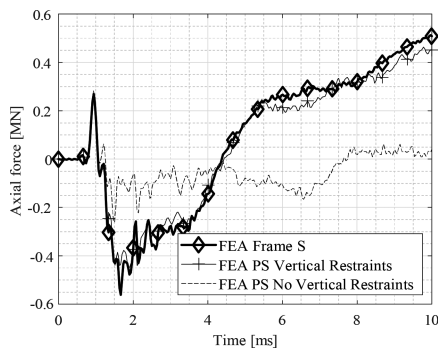


Figure 6. The variation of the axial force in time for the models.

Figure 7 shows the plastic strains for the concrete and reinforcement in the FEA Frame S model and the FEA PS Vertical Restraints model. The figures showing the plastic strain in the concrete are configured in such way that the dark grey elements show cracks that are fully opened. The plots for reinforcement plastic strain use an arbitrarily low limit implying that black elements have undergone plastic deformation, and the annotations show on which side of the flexural reinforcement this occurs. Figure 7(a) and (b) indicate similar crack patterns, where the main difference is the larger crack distribution possible in the frame models. This further contributes to the higher stiffness previously observed. A similar phenomenon is shown in (c) and (d); the spread of the plastic hinges at the supports and in the field is much larger for the frame model, implying a larger total moment that decelerates the wall in the frame model, thus resulting in the reduced maximum amplitude. A better model for the design would therefore have used a larger equivalent width of the plate strip.

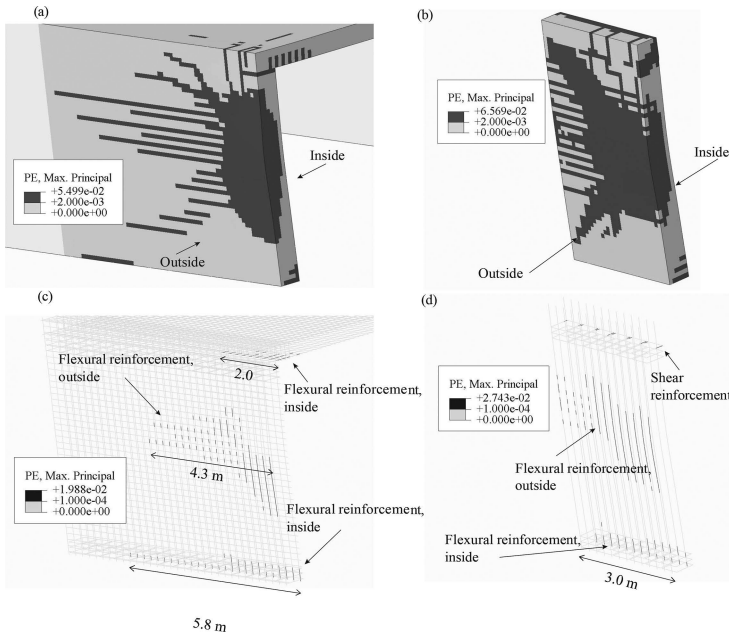


Figure 7. Maximum principal plastic strain at the time of maximum displacement for: (a) concrete in the FEA Frame S model; (b) concrete in the FEA PS Vertical Restraints model; (c) reinforcement in the FEA Frame S model; and (d) reinforcement in the FEA PS Vertical Restraints model.

4.2 Results from the gas explosion analyses

Figure 8(a) and (b) show how the overpressure $P^+(t)$ varies over time t at the three monitor points for both gas explosion models. Due to resource limitations, the hydrogen gas model could be analyzed to about 110 ms before being cancelled, and the propane gas model to about 300 ms. The same time span and overpressure limits are used in both figures, meaning that their shape can be directly compared. The cloud containing an air-hydrogen gas mixture in (a) shows significant overpressures at an earlier point in time when compared to the air-propane gas mixture in (b), indicating a higher average flame velocity. The maximum amplitudes in (a) are, therefore, larger than those in (b) as the flame velocity and overpressure level are coupled. As shown in (c), the larger maximum amplitude $P_{\max}^+(R)$ of the hydrogen gas model seems to hold until a distance from the ignition point of about 26 m; thereafter, the measured values of overpressure are similar for both gas types. The large overpressure measured in (a) implies that a DDT might occur, but this transition cannot accurately be captured by FLACS-CFD. The waveform in (a) implies a strong deflagration or a detonation, and the waveform in (b) corresponds to a strong deflagration with a small probability of DDT.

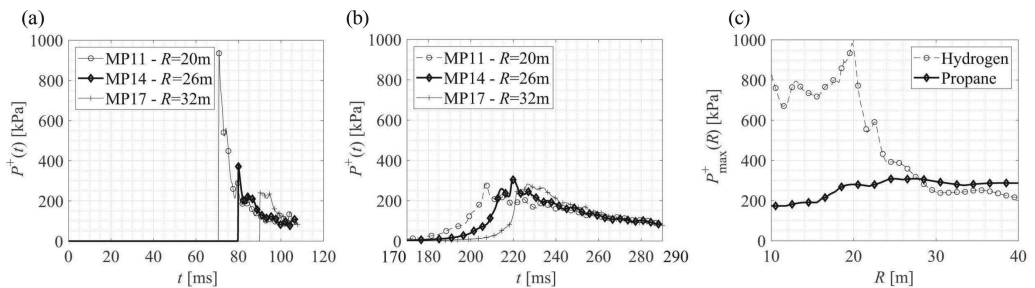


Figure 8. (a) $P^+(t)$ for the hydrogen gas cloud model; (b) $P^+(t)$ for the propane gas cloud model; and (c) $P_{\max}^+(R)$ for both models.

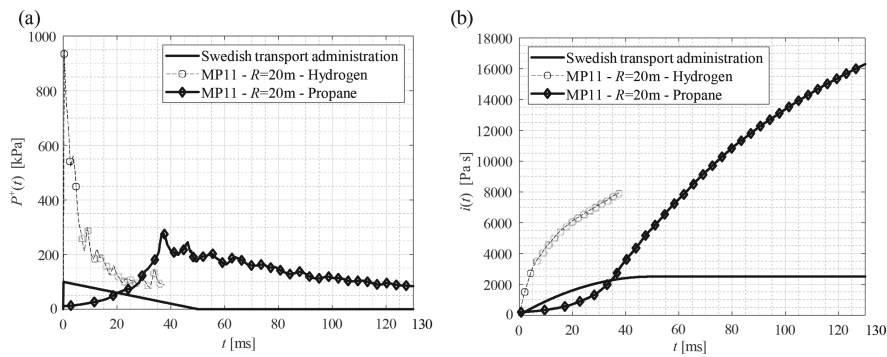


Figure 9. (a) $P^+(t)$ for both numerical models and due to the uniform pressure from Table 1; and (b) $i(t)$ for both models and due to the uniform pressure from Table 1.

Figure 9(a) and (b) compare the results determined by the gas explosion analyses to the design provisions in the Swedish Transport Administration (2021). The load used for comparison is the uniform pressure in the traffic space in Table 1, as this is comparable to the pressure measured further down in the tunnel space without reflection, similar to the positions of the monitor points in the simulations. This accidental load is a general load used for design, and not specific for gas explosions. The local pressure in Table 1 that was used for design is similar to a reflected blast close to the ignition point, and the results at such points in the simulations were deemed to not be accurately determined as the DDT could not be captured accurately by the software used for simulation. A combination of the intensity of both the overpressure $P^+(t)$ and impulse intensity $i(t)$ is what governs the response as described in the Swedish Fortification Agency (2011), meaning that both are analyzed. To simplify comparison, $P^+(t)$ have been moved in time to initiate simultaneously. In (a), the maximum amplitude using the design provisions show to be smaller than that determined by the simulations, as this corresponds to a weaker deflagration, and the duration is also smaller. This results in a lower impulse intensity as shown in (b). Transportation of the substances considered, therefore, results in the need for additional analyses. If in (b) the results of the hydrogen gas explosion are interpolated, it seems like the propane gas results in a larger impulse intensity although its maximum amplitude of the overpressure is significantly smaller.

5 CONCLUSIONS

The design provision showed a need for shear reinforcement, but the finite element analyses showed a negligible effect of it. This was shown to be an effect of a conservative prediction of the support reaction for load cases of small durations in relation to the wave propagation velocity in the element. The design method used for the wall showed to be conservative in terms of predicting the maximum displacement. A larger equivalent width of the plate strip model would have resulted in a more realistic response. The occurrence of axial forces in the models showed to occur, both with and without vertical restraint. This should be further investigated.

The gas explosion analysis of a hydrogen cloud showed a higher average flame speed and larger maximum overpressure levels when compared to the analysis containing propane. This is due to the increased reactivity which, possibly, led to a DDT for the hydrogen cloud. There was an indication of a larger maximum impulse intensity of the gas cloud containing propane. The results of the simulations indicate more severe load parameters compared to the design provisions for monitor points further down the tunnel. This indicates the need of performing special inquiry for transport of such substances. Conclusions regarding pressure levels close to the ignition point could not be deduced as the results were uncertain due to possible DDT.

REFERENCES

- van der Berg, A.C. 1985. The multi-energy method - A framework for vapour cloud explosion blast prediction. *Journal of hazardous materials* 12: 1–10.
- Biggs, M. J. (1st) 1964. *Introduction to structural dynamics*. New York: McGraw-Hill.
- Bjerkevedt, D., Bakke, J.R. & Wingerden, K. (1st.) 2000. *Gas explosion handbook*. Bergen: Gexcon AS.
- CEN. 2005. *Eurocode 2: Design of Concrete Structures – Part 1-1: General Rules and Rules for Buildings*. Belgium: European Committee for Standardization.
- Cornelissen, H., Hordijk, D. & Reinhardt, H. 1986. Experimental determination of crack softening characteristics of normal weight and lightweight concrete. *Heron* 31(2): 45–56.
- Dassault Systèmes. 2014. *ABAQUS/Standard User's Manual, Version 6.14*. United States: Dassault Systèmes Simulia Corp.
- von Essen, W. 1973. *Anvisningar för dimensionering av armerade betongkonstruktioner som skydd mot verkan av konventionella vapen inom närmissionsområde*. Stockholm: Fortifikationsförvaltningen.
- FIB. 2013. *fib Model Code for Concrete Structures 2010*. Berlin: Wilhelm Ernst & Sohn.
- Gexcon AS. 2022. *FLACS-CFD v22.1 User's Manual*. Bergen: Gexcon AS.
- Magnusson, J. 2019. *Shear in concrete structural elements subjected to dynamic loads*. PhD Thesis, KTH Royal Institute of Technology, Stockholm.
- Mathern, A. & Yang, J. 2021. A Practical Finite Element Modeling Strategy to Capture Cracking and Crushing Behavior of Reinforced Concrete Structures. *Materials* 14: 1–24.
- Oran, E.S, Chamberlain G. & Pekalski, A. 2020. Mechanisms and occurrence of detonations in vapour cloud explosions. *Progress in energy and combustion science* 77: 1–37.
- Strehlow, R. 1998. Unconfined vapour cloud explosions - An overview. *Fourteenth symposium (international) on combustion; Symposium (International) on Combustion, Pennsylvania, 20-25 August 1997*. Amsterdam: Elsevier.
- Swedish Fortifications Agency. 2011. *Fortifikationsverkets konstruktionsregler FKR 2011*. Stockholm: Fortifikationsverket.
- Swedish Transport Administration. 2021. *Krav tunnelbyggande*. Stockholm: Trafikverket.
- Swedish Transport Administration. 2020. *Krav vägar och gators utformning*. Stockholm: Trafikverket.